# Influence of grain boundaries on the magnetization reorientation transition in ultrathin films

G. Rodary,[1] V. Repain,[1] R. L. Stamps,[2] Y. Girard,[1] S. Rohart,[1] A. Tejeda,[1] and S. Rousset[1]
[1]*Laboratoire Matériaux et Phénomènes Quantiques, Université Paris 7, UMR CNRS 7162, Case 7021, 2 Place Jussieu, 75251 Paris, France*
[2]*School of Physics M013, University of Western Australia, 35 Stirling Highway, Crawley WA 6009, Australia*
(Received 8 January 2007; published 16 May 2007)

A magnetic reorientation transition is studied *in situ* in model experimental systems of Co grown on Au(111) and Au(788). Results from magneto-optic measurements and scanning tunneling microscopy, obtained on these two different self-ordered systems, demonstrate that grain boundaries formed during the film growth strongly influence the magnetic properties of the films. The nanometer scale of the magnetization reversal at the transition makes the temperature an essential parameter to predict experimental features observed in the magnetic reorientation transition.

DOI: 10.1103/PhysRevB.75.184415 PACS number(s): 75.70.Ak, 68.37.Ef, 68.55.Jk, 75.75.+a

The formation of perpendicular magnetic anisotropy in ultrathin films is an important problem in terms of application for high-density data storage and also as a test of predictive quantum materials theory.[1,2] An important goal is to understand and control magnetic anisotropy in transition-metal magnetic structures. The microscopic origin of magnetic anisotropy involves intricate relationships between magnetic properties and structural parameters. Magnetic anisotropy in magnetic thin films can be modified through crystal structure,[3] film thickness,[4] temperature,[5] and step densities.[6–8] The surface anisotropy, which can be in-plane or out-of-plane anisotropy, plays an important role in such systems and leads to specific orientation of the film magnetization.[9] Very often, these systems support large lattice mismatches that induce grain-boundary formation during the first stage of growth. The purpose of this paper is to use accurately determined magnetic film morphology, deduced from scanning tunneling microscopy images, in order to determine how the magnetization orientation is influenced by the density and distribution of grain boundaries.

The magnetic reorientation transition (MRT) observed in many magnetic ultrathin films appears as a change of the magnetization orientation as a function of the film thickness. When the magnetic surface anisotropy is out of plane, the magnetocrystalline anisotropy at the interface tends to orient the magnetization perpendicular to the plane of the film, whereas the dipolar magnetic interaction favors an in-plane orientation. Therefore, at a critical thickness $t_c$, one observes the MRT from an out-of-plane to an in-plane direction. Interestingly, there have been very few experiments able to explore and demonstrate how structural imperfections can influence magnetic anisotropy and MRT.[10] However, few theoretical works have pointed out the importance of a noncollinear magnetization due to structural inhomogeneities for the magnetism of ultrathin films.[11,12] We propose in this paper a direct link between the granular structure of the film and the mechanism of the MRT. The grains induce the presence of a magnetic volume, directly linked to the grain size, that makes the temperature more significant for the MRT.

The system of Co on Au is advantageous for experimental studies of grain-boundary formation. Both elements are immiscible, and the large 14% lattice mismatch causes the Co to relax after the first monolayers (ML). Moreover, the film growth occurs through the merging of self-organized structures on the Au surface. This forms a grain-boundary network. In order to obtain films with different grain-boundary densities and to avoid uncontrolled modification of the magnetic anisotropy through temperature-dependent magnetoelastic effects,[13] we have grown Co films under the same conditions but on different naturally patterned substrates. The nucleation density of Co clusters on Au(788) (Ref. 14) is about four times that found for growth on Au(111).[15] This provides a simple way of obtaining two different grain-boundary densities.

Samples have been prepared in an ultrahigh vacuum chamber with a base pressure $<5\times10^{-11}$ mbar. Au surfaces are etched by 900 eV argon-ion sputtering and then annealed at 800 K. Surface cleanness is controlled by Auger spectrometry and scanning tunneling microscopy (STM) images. The Co is evaporated at 300 K with a typical growth rate of 0.1 ML/min under a pressure $<1\times10^{-10}$ mbar. Co thickness is controlled *in situ* by Auger spectrometry measuring the relative intensity of Co(53 eV) and Au(69 eV) Auger peaks, previously calibrated by Rutherford backscattering spectrometry measurements. Polar magneto-optical Kerr effect (MOKE) can be performed *in situ* during growth. Magnetization hysteresis loops are stored every 20 s with a 0.4 Hz field sweep rate (for a maximum magnetic field of 600 mT). A loop is taken typically every 0.03 ML with a negligible error on thickness associated with the measurement time during one cycle.

STM images of the Co growth on Au(111) and Au(788) at room temperature and for different Co thicknesses are shown in Fig. 1. The grain boundaries form during the growth of the very first layers of Co, and the nucleation densities are controlled by the surface geometries. Co on Au(111) nucleates at the elbows of a herringbone pattern reconstruction,[15] whereas nucleation sites are situated at the junction of the discommensuration lines and the step edges for Au(788).[14]

In both cases, nucleation of clusters is periodic, but with a higher density of Co islands on Au(788) (see schematic in Fig. 1). 2 ML high dots self-organize and some of them begin to coalesce at a Co coverage of 1 ML [Figs. 1(a) and 1(b)], although the majority of dots remain separated by thin trenches. Trenches form because of the first Co atomic layer

 

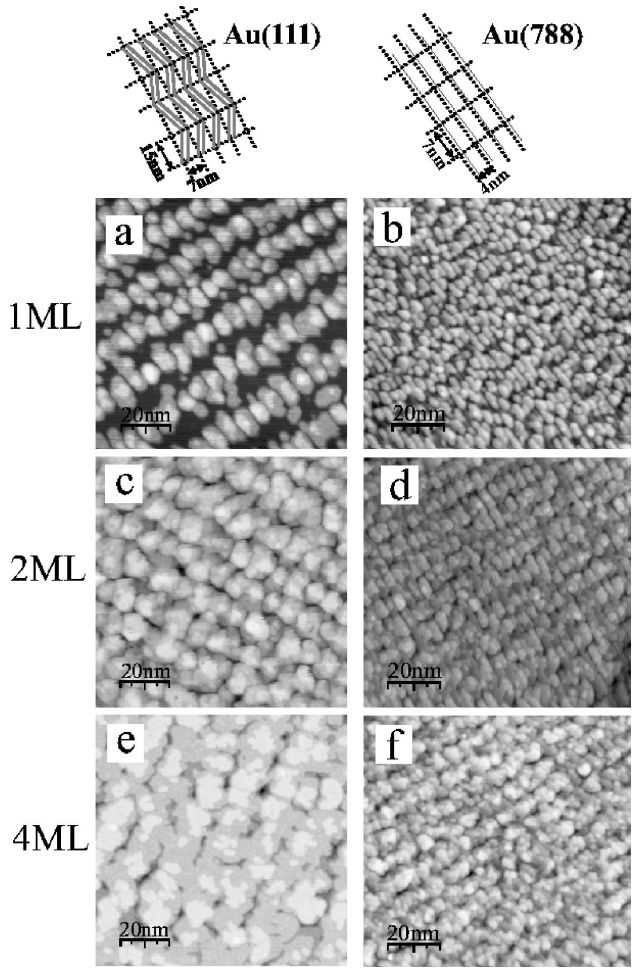


FIG. 1. STM images of Co/Au(111) (left) and Co/Au(788) (right) for 1 ML [(a) and (b)], 2 ML [(c) and (d)], and 4 ML [(e) and (f)]. The drawings represent the unit cells of the Co dot arrays delimited by herringbone on Au(111) and separated by step edges on Au(788).

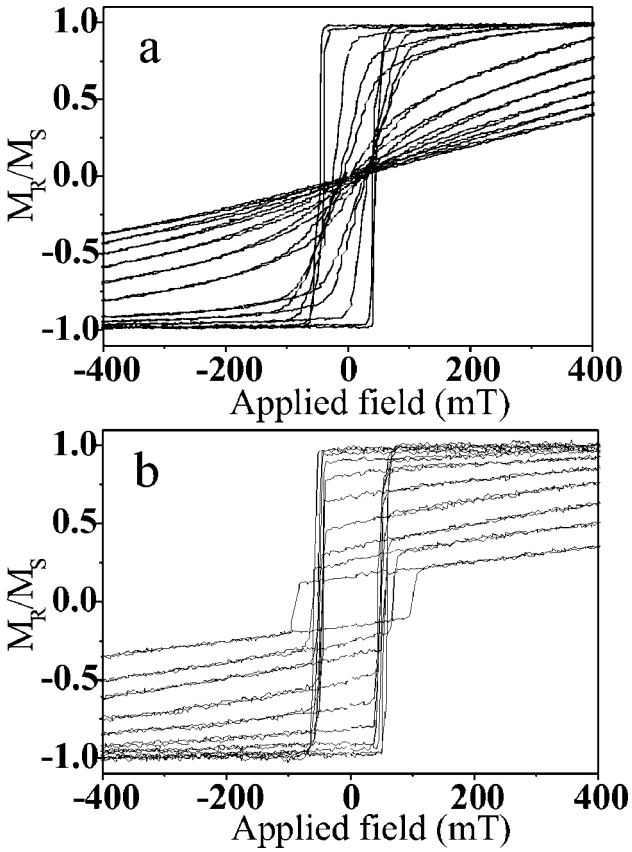


FIG. 2. Raw hysteresis loops stored during the reorientation transition for Co/Au(111) (a) and Co/Au(788) (b). Each 0.1 ML step are shown from 4 to 5 ML for Au(111) and from 2.5 to 3.5 ML for Au(788).

relaxation, i.e., two neighboring dots cannot coalesce without forming an atomic random phase domain boundary. Even for a coverage above the percolation threshold, at 2 ML, these defects remain and the formation of a grain boundary network based on the trenches can be seen in the images in Figs. 1(c) and 1(d). At 4 ML [Figs. 1(e) and 1(f)], STM images show an established network of grain boundaries following the pattern of the initially nucleated dot array although we can observe occasionally the merging of two neighboring grains. Finally, the continuous film consists of different grains separated by grain boundaries with a density controlled by the initial nucleation pattern. Previous x-ray studies on Co/Au(111) (Ref. 16) and Co/Au(788) (Ref. 17) ultrathin films strongly support this conclusion.

Magnetic properties of these films were studied using *in situ* MOKE hysteresis loops, from the first detectable signal (~0.5 ML) up to 10 ML thick films. A polar configuration was used to measure the out-of-plane component of the magnetization. Hysteresis cycles close to the MRT are shown in Fig. 2 for each 0.1 ML coverage of Co/Au(111) and Co/Au(788). During the MRT, hysteresis loops change from open square cycles to closed cycles, and the remanent magnetization $M_R$ decreases as expected. Note that for the Co/Au(788) films at high thickness, the loops remain open for a decreasing part of the total magnetization. However, we always reach a reversible part of the loop and the measured remanent magnetization is therefore not dependent on our maximum available field.

Variation of $M_R$ normalized to the saturation magnetization $M_S$ was determined for each coverage. When the magnetization is out of plane, i.e., for square cycles, the sample can be saturated. The saturated magnetization $M_S$ is measured directly and shows a perfect linear dependence on the film thickness. This allows $M_S$ to be extrapolated to all thicknesses and $M_R/M_S$ versus film thickness can be determined. Results are shown in Fig. 3(a) for both samples. A value of unity corresponds to a magnetization perpendicular to the sample plane, and $M_R/M_S=0$ corresponds to a magnetization lying in plane. A critical thickness $t_c$ exists at the reorientation transition where the magnetization is at $\pi/4$ of the normal direction. A value of $t_c=4.23$ ML for Co/Au(111) was found, in good agreement with previous data[18,19] and $t_c=2.95$ ML for Co/Au(788). Moreover, we note that Beauvillain *et al.* have measured the thickness dependence shape for sandwich samples Au/Co/Au(111) with some hint of similar features.[19]

The significance of the present results is that the high

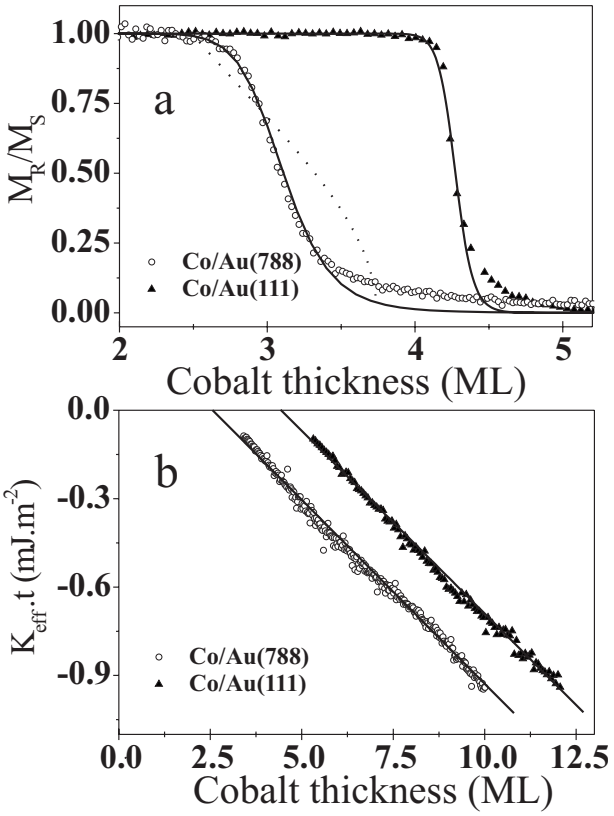


FIG. 3. (a) Residual magnetization at zero field versus Co thickness for Au(788) surface (open circle) and Au(111) surface (dark triangle). The solid lines correspond to the model described in the text, the dotted line to the Stoner-Wohlfarth model. (b) Thickness variation of the effective anisotropy and linear fits for both samples.

quality of the data and the large number of points allow tests of models describing the MRT. To get a continuous variation of the magnetization during the MRT, as determined experimentally, one generally considers anisotropy terms of the first and second order and of opposite signs in the Stoner-Wohlfarth Hamiltonian.[20] The second-order anisotropy is generally attributed to finite temperature or noncollinearity of the magnetization and is used as a phenomenological parameter to adjust the width of the MRT.[18,21] This common model assumes coherent rotation without thermal activation. We have plotted with a dotted line in Fig. 3(a) the fit of the experimental data with this model. We can observe the very poor accuracy of this plot with a wrong concavity as compared to the measured MRT. This motivates the proposal of a more realistic model.

In the following, we propose an alternative model for the MRT based on our morphological observations. Because grain boundaries exist, as observed by STM, they should influence the magnetic properties of the film. Indeed, the ferromagnetic order is highly susceptible to any fluctuations close to the MRT and noncollinear magnetic structures are very likely to occur. In the present system, the network of grain boundaries induces a strong local variation of either the magnetic exchange or anisotropy. Indeed, as sketched in Fig. 4, the interatomic distance can be drastically different at the grain boundary, and it is well known that magnetic exchange

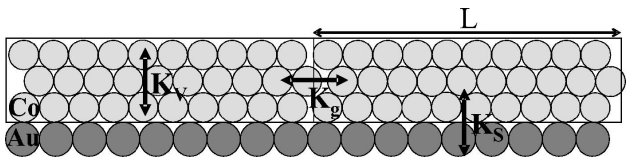


FIG. 4. Schematic of magnetic anisotropies. A schematic of the Co film structure highlights the periodic phase grain boundary.

and anisotropy are very sensitive to the interatomic distance. The details of a model that considers these periodic variations are beyond the scope of this paper. However, it is worthy to note that the influence of a nonuniform anisotropy on the magnetic structure of ultrathin films has been studied theoretically and can lead to magnetic ripples and high-order terms in the averaged magnetic anisotropy.[11,22] The important point is that the local variations of exchange and anisotropy can be dominant near the MRT and induce a strong noncollinear magnetization. The natural length scale of the grains can have its magnetic counterpart, i.e., domain walls located at the grain boundaries, separating out-of-plane and in-plane domains. This induces two magnetic orientations possible at equilibrium, and these can be separated in energy by an activation barrier.

The MRT is defined as the transition between these two possible magnetic orientations. The energy difference between these two states at remanence is given by the anisotropy energy between the hard and easy axes. This assertion is not trivial for domains at the nanometer scale and should be refined by a complete calculation of the magnetization in a model with local variations of exchange and anisotropy at the grain boundaries. However, it certainly gives a good order of magnitude of the energy difference between out-of-plane and in-plane domains. At finite temperatures, the equilibrium value of the average out-of-plane component of the magnetization, $M_R$, can be found by solving a master rate equation using thermal occupation probabilities for the two orientations. These probabilities depend on the energy barrier between the two states. However, the steady-state solution can be obtained by considering only the statistical thermal occupation of the out-of-plane ($n_\uparrow$) and in-plane ($n_\rightarrow$) magnetic grains. $n_\rightarrow/n_\uparrow$ is given by the usual Boltzmann factor considering the energy difference between these two states. Finally, $M_R/M_S=n_\uparrow/n_\uparrow+n_\rightarrow=[1+\exp(-K_{eff}V/kT)]^{-1}$, where $V$ is a "magnetic volume" and $K_{eff}$ is the associated effective anisotropy. In contrast to a Stoner-Wohlfarth model, the broadening of the transition is now given by the temperature and the magnetic volume due to the grains. The physical meaning of this result is that the grains size, i.e., the structural inhomogeneity of the magnetic film caused by grain boundaries, induces the presence of a new characteristic volume, or length, that is added to the common exchange length. This relation can now be used to fit our $M_R/M_S(t)$ variation, taking into account the grain sizes.

In order to compare our model to the data presented in Fig. 3(a), we determine the thickness variation of the effective anisotropy $K_{eff}$ for both samples. When the external field is applied parallel to the hard axis direction, the magnetization reversal can be understood by a simple coherent magnetization rotation with a total energy $E=K_{eff}\sin^2\theta$

$-\mu_0 MH\cos\theta$. Experimentally, we extract the saturation field $2K_{eff}/M_S$ for cycles above $t_c$ from their slope, and the saturated magnetization calibration done with saturated cycles.[20] The resulting thickness ($t$) variation of $K_{eff}$ times $t$ is shown in Fig. 3(b). It follows almost perfectly the usual relation used for ultrathin films $K_{eff}=K_V+K_S/t$, where $K_V=K_{MC}-\mu_0 M_S^2/2$ is the sum of the magnetocrystalline anisotropy and the shape anisotropy, and $K_S$ is the interface anisotropy. The intercept and the slope deduced from Fig. 3(b) provide values for $K_S=0.55\pm0.01$ mJ m$^{-2}$ and $K_V=-622\pm5$ kJ m$^{-3}$ for Co/Au(111) and $K_S=0.32\pm0.01$ mJ m$^{-2}$ and $K_V=-624\pm5$ kJ m$^{-3}$ for Co/Au(788) using the bulk value for $M_S$. The values of volume and surface anisotropy terms for Co/Au(111) are in very good agreement with other values in the literature.[19,21,23] Using these experimental determinations of $K_{eff}$ for both samples, we can compare our model and the data using the magnetic volume involved in the MRT of each sample as the only free parameter. Figure 3(a) shows the results of the model by a continuous line for both systems. We recall that the result from the coherent rotation model with a phenomenological second-order anisotropy $K_2$ is also shown as a dotted line around the MRT of Co/Au(788). In this case, the magnetization, if $M_R<M_S$, follows the expression $M_R/M_S=[1+(K_V+K_S/t)/(2K_2)]^{1/2}$, where $K_2$ is taken from Ref. 21. The thermal broadening model is in very good agreement with the data points, in contrast to the coherent rotation model. We extract the magnetic volumes from the fit of the experimental curves by our model. These volumes correspond to a surface at the transition thickness, whose square root can be easily compared to STM images. The domain size corresponding to the activation magnetic volumes found from the fit are $27\pm5$ nm for Au(111) and $14\pm2$ nm for Au(788). These sizes are very similar to what is deduced from the morphology shown in Figs. 1(e) and 1(f). This observation strengthens the assumption that grain boundaries, as any other structural inhomogeneities, have a strong influence on the magnetism close to the MRT. Note that these magnetic lateral sizes are too small to be resolved experimentally by scanning electron microscopy with polarization analysis.[10]

In conclusion, we have used two different substrates and self-ordered growth in order to control the density of grain boundaries into Co films deposited on Au. High-accuracy experimental data of the MRT demonstrate that the usual model of coherent rotation of the magnetization at 0 K cannot be used at least for Co/Au ultrathin films. We propose an alternative model that takes into account the grain boundaries as an energy barrier between out-of-plane and in-plane magnetic domains. This implies a change in local magnetization configurations around the MRT and the presence of a characteristic magnetic volume directly caused by the morphological properties. The magnetization reversal at the MRT can then occur through thermally activated reversal of these very small volumes related to the structural inhomogeneity of the film. This induces a thermal broadening of the MRT, in agreement with our observed remanent magnetization variation with thickness. The fitted magnetic volumes are in good agreement with grain sizes imaged by STM, showing the direct link between morphological properties of the film and its magnetic behavior. This demonstrates that the structural imperfections of magnetic ultrathin films such as grain boundaries strongly influence the MRT.

This research was supported by a French ACI. R.L.S. gratefully acknowledges support from Paris VII and the Australian Research Council.

[1] P. F. Carcia, A. D. Meinhaldt, and A. Suna, Appl. Phys. Lett. **47**, 178 (1985).
[2] C. Chappert, K. L. Dang, P. Beauvillain, H. Hurdequint, and D. Renard, Phys. Rev. B **34**, 3192 (1986).
[3] O. Eriksson, B. Johansson, R. C. Albers, A. M. Boring, and M. S. S. Brooks, Phys. Rev. B **42**, 2707 (1990).
[4] W. Weber, C. H. Back, A. Bischof, C. Wursch, and R. Allenspach, Phys. Rev. Lett. **76**, 1940 (1996).
[5] W. Wulfhekel, S. Knappmann, B. Gehring, and H. P. Oepen, Phys. Rev. B **50**, 16074 (1994).
[6] M. Albrecht, T. Furubayashi, M. Przybylski, J. Korecki, and U. Gradmann, J. Magn. Magn. Mater. **113**, 207 (1992).
[7] J. Chen and J. L. Erskine, Phys. Rev. Lett. **68**, 1212 (1992).
[8] H. J. Choi, Z. Q. Qiu, J. Pearson, J. S. Jiang, D. Li, and S. D. Bader, Phys. Rev. B **57**, R12713 (1998).
[9] H. Fritzsche, H. J. Elmers, and U. Gradmann, J. Magn. Magn. Mater. **135**, 343 (1994).
[10] M. Speckmann, H. P. Oepen, and H. Ibach, Phys. Rev. Lett. **75**, 2035 (1995).
[11] B. Dieny and A. Vedyayev, Europhys. Lett. **25**, 723 (1994).
[12] P. J. Jensen and K. H. Bennemann, Surf. Sci. Rep. **61**, 129 (2006).
[13] S. Padovani, F. Scheurer, I. Chado, and J. P. Bucher, Phys. Rev. B **61**, 72 (2000).
[14] V. Repain, G. Baudot, H. Ellmer, and S. Rousset, Europhys. Lett. **58**, 730 (2002).
[15] B. Voigtländer, G. Meyer, and N. M. Amer, Phys. Rev. B **44**, 10354 (1991).
[16] O. Fruchart, G. Renaud, A. Barbier, M. Noblet, O. Ulrich, J.-P. Deville, F. Scheurer, J. Mane-Mane, V. Repain, G. Baudot, and S. Rousset, Europhys. Lett. **63**, 275 (2003).
[17] F. Leroy, Ph.D. thesis, University of Grenoble, 2004.
[18] R. Allenspach, M. Stampanoni, and A. Bischof, Phys. Rev. Lett. **65**, 3344 (1990).
[19] P. Beauvillain, A. Bounouh, C. Chappert, R. Mégy, S. Ould-Mahfoud, and J. P. Renard, J. Appl. Phys. **76**, 6078 (1994).
[20] E. C. Stoner and E. P. Wohlfarth, Philos. Trans. R. Soc. London, Ser. A **240**, 599 (1948).
[21] L. Cagnon, T. Devolder, R. Cortes, A. Morrone, J. E. Schmidt, C. Chappert, and P. Allongue, Phys. Rev. B **63**, 104419 (2001).
[22] J. C. Slonczewski, Phys. Rev. Lett. **67**, 3172 (1991).
[23] V. Grolier, J. Ferré, A. Maziewski, E. Stefanowicz, and D. Renard, J. Appl. Phys. **73**, 5939 (1993).